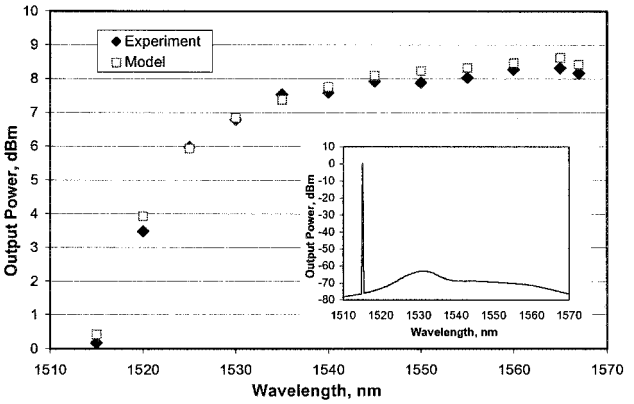

Figure 3 Tuning characteristics of Er^{3+}-doped fiber ring laser. Inset: a numerical spectral plot tuned at 1515 nm. Notice a small hump in the 1530 nm region having a similar profile as in Figure 4 (arrow)

Tuning the laser to a wavelength shorter than 1535 nm brings about a significant drop in the output power level; see Figure 3. The drop in power level is due to higher intracavity losses incurred by the variation of the insertion loss of the tunable filter. The plot shows the continuous tuning characteristic of the laser, with small power variations in the 1535–1567 nm tuning range. Under certain conditions, with regard to its intracavity loss, output coupler ratio, and EDF length, an EDFL (without a filter in the cavity) will lase in either the 1530 or 1550 nm region, but not in the 1540 nm region. However, the laser with a filter incorporated in the cavity can be tuned and lase at 1540 nm. A numerical study shows that the filter functions such that only modes within the filter bandwidth are allowed to oscillate and are amplified; hence, all of the power is pumped and channeled into the tuned bandwidth. A numerical spectral plot of the laser output tuned at 1515 nm is shown in the inset of Figure 3. A small hump in the 1530 nm region, which illustrates a higher amplified spontaneous emission (ASE) level that results from high absorption and gain coefficient at 1530 nm, demonstrates a similar profile (arrow) in Figure 4. The numerical plot shows a close match with the measured result. The measured output spectra of the EDFL tuned from 1515 to 1567 nm are shown in Figure 4, with a signal-to-noise ratio (SNR) of about 70 dB. The tuning limitation of the filter restrains further measurement beyond 1567 nm, although the plots in Figures 3 and 4 show relatively high output power in this region. Numerical results show that the output power drops substantially when the laser is tuned to 1570 nm and at a longer wavelength. Photon reabsorption and emission to a longer wavelength could not be realized due to the short length of EDF used. At 12 m length of EDF, the model shows that the laser exhibits a relatively high output power when tuned at 1575 nm.

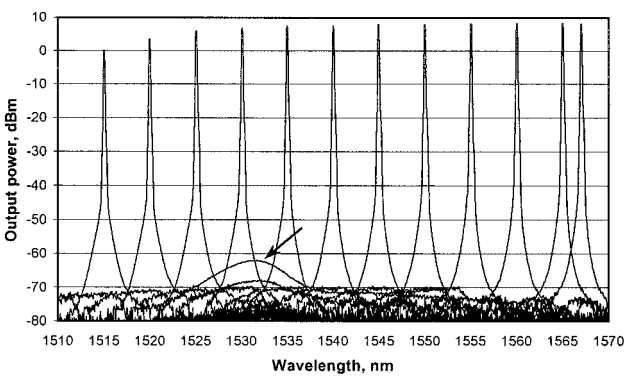

Figure 4 EDFL output spectra when tuned from 1515 to 1567 nm. The 3 dB spectral width is 0.044 nm, limited by the optical spectrum analyzer resolution bandwidth

4. CONCLUSION

We have demonstrated a tuning range of more than 50 nm from an all-fiber ring erbium-doped fiber laser with an SNR of 70 dB. This tunable laser source can be used for wavelength-division multiplexed systems. A numerical model was briefly discussed and used to compare measured and calculated results. The experimental results have good matching values with the modeled results.

REFERENCES

1. Y.T. Chieng, G.J. Cowle, and R.A. Minasian, Optimization of wavelength tuning of erbium-doped fiber ring lasers, J Lightwave Technol 14 (1991), 1730–1739.
2. A. Frenkel and C. Lin, Inline tunable etalon filter for optical channel selection in high density wavelength division multiplexed fibre systems, Electron Lett 24 (1988), 159–161.
3. C.Y. Chen, M.M. Choy, M.J. Andrejco, M.A. Saifi and C. Lin, A widely tunable erbium-doped fiber laser pumped at 532 nm, IEEE Photon Technol Lett 2 (1990), 18–20.
4. J.L. Zyskind, J.W. Sulhoff, J. Stone, D.J. DiGiovanni, L.W. Stulz, H.M. Presby, A. Piccirilli, and P.E. Pramayon, Electrically tunable, diode-pumped erbium-doped fibre ring laser with fibre Fabry-Perot etalon, Electron Lett 27 (1991), 1950–1951.
5. H. Schmuck, Th. Pfeiffer, and G. Veith, Widely tunable narrow linewidth erbium doped fibre ring laser, Electron Lett 27 (1991), 2117–2119.
6. B. Pederson, A. Bjarklev, J.H. Povlsen, K. Dybdal, and C.C. Larsen, The design of erbium-doped fiber amplifiers, J Lightwave Technol 9 (1991), 1105–1112.
7. S. Selvakennedy, M.A. Mahdi, M.K. Abdullah, P. Poopalan, and H. Ahmad, Design optimisation of erbium-doped fibre ring laser through numerical simulation, Opt Commun 170 (1999), 247–253.

HILBERT CURVE FRACTAL ANTENNA: A SMALL RESONANT ANTENNA FOR VHF/UHF APPLICATIONS

K. J. Vinoy,[1] K. A. Jose,[1] V. K. Varadan,[1] and V. V. Varadan[1]
[1] Center for the Engineering of Electronic and Acoustic Materials and Devices
The Pennsylvania State University
University Park, Pennsylvania 16802

Received 28 November 2000

ABSTRACT: *The usefulness of fractal Hilbert curves in antenna geometry is explored here for the first time. Apart from being simple and self-similar, these curves have the additional property of approximately filling a plane. These properties are exploited in realizing a "small" resonant antenna. This approach has resulted in an antenna size smaller than λ / 10 and still resonant, with performance comparable to a dipole*

whose resonant length is close to λ / 2. Numerical predictions of the input impedance of the antenna have been compared with experiments. The effect of additional fractal iterations on the reduction of the resonant frequency has been studied. The radiation characteristics of the antenna at the resonant frequencies provided show that this is very similar to the dipole characteristics. © 2001 John Wiley & Sons, Inc. Microwave Opt Technol Lett 29: 215–219, 2001.

Key words: *fractal antennas; Hilbert curves; multiband antennas; small antennas*

INTRODUCTION

With the widespread proliferation of telecommunication technology in recent years, the need for small-size multiband antennas has increased manifold. However, an arbitrary reduction in the antenna size would result in a large reactance and deterioration in the radiation efficiency. Meander-line and zig-zag antennas have been studied for their capability in antenna size reduction [1, 2]. However, novel antenna configurations using fractal Hilbert curves introduced here can reduce the antenna size further. Once optimized for radiation characteristics, these antennas can find many applications in UHF/VHF communication antennas.

Two important properties of fractal patterns are self-similarity and scale invariance [3]. Fractals consist of identical or similar elements repeated in different magnifications, orientations, and positions, most often in an interconnected fashion to obtain the final structure. The seemingly random nature of fractals is exploited in several fields of engineering and science. Jaggard and Spielman [4] have shown that the geometric similarity of fractals can be translated to their electromagnetic behavior, in the context of diffraction studies. Similarly, the diffracted fields of self-similar fractal screens are also found to be self-similar [5]. Although a large number of fractal patterns have been studied in mathematics, only very of few of these have actually been implemented for antenna structures. Among those currently reported in the literature include Koch curves and the Sierpinski gasket [6, 7]. Some of these geometries have recently been pursued for antenna applications because of their inherent multiband nature. However, incorporation of many new fractal geometries into the antenna structures, and various aspects of their optimization, are still in the incipient stages. Nonetheless, the analysis of fractal distribution of elements in antenna arrays has been extensively studied [8].

The fractal antennas using a Siepinski gasket have been configured to obtain multiple-frequency bands [9]. These antennas resonate at frequencies in a near-logarithmic interval. The individual bands at these resonant frequencies are generally small. However, their relative positions can be controlled by perturbing the shapes of the fractal geometry of the antenna configuration [10]. This approach has resulted in a multiband antenna with the individual bands located almost arbitrarily. Apart from this, other important features of this fractal antenna include low profile, the possibility of multiple frequency bands, and moderate gain. The gain of this antenna is quite promising, considering its overall size. These have been extended further to make them wideband and conformal [11].

In this paper, we present a new set of fractal patterns which are used here in antenna design for the first time. These consist of Hilbert curve patterns, which have several important characteristics hitherto unexplored in antenna engineering.

FRACTAL HILBERT CURVES

Various iteration stages of fractal Hilbert curves are shown in Figure 1. It may be observed that geometry at a stage can be obtained by putting together four copies of the previous iteration, connected to additional line segments. For example, the geometry of order 2 can be thought of as four copies of the geometry with order 1 (arranged in different orientations), connected to the additional segments shown with dashed lines.

It would be interesting to identify the fractal properties of this geometry. The plane-filling nature is evident by comparing the first few iterations of the geometry shown in Figure 1. It may, however, be mentioned that this geometry is not strictly self-similar since additional connection segments are required when an extra iteration order is added to an existing one. But the contribution of this additional length (shown with dashed lines in Fig. 1) is small compared to the overall length of the geometry, especially when the order of the iteration is large. Hence, this small additional length can be disregarded, which makes the geometry self-similar.

A similar ambiguity also prevails in determining the dimension of the geometry. The topological dimension of the curve is 1 since it consists only of line segments. However, the dimension of a fractal curve can be defined in terms of a multiple-copy algorithm [12]. The similarity dimension D is defined as

$$D = \frac{\log(N)}{\log(1/f)}$$

where N is the number of copies and f is the scale factor of consecutive iterations. The dimension of the Hilbert curve is

$$D = \frac{\log[(4^n - 1)/(4^{n-1} - 1)]}{\log[(2^n - 1)/(2^{n-1} - 1)]}$$

$$\approx (\text{for large } n)\frac{\log(4^n/4^{n-1})}{\log(2^n/2^{n-1})} = \frac{\log 4}{\log 2} = 2.$$

The similarity dimension of this curve approaches an integer value (2) because of the approximation involved when a large fractal order is considerd. But if we consider the length and number of line segments first and second iterations, the dimension is

$$D_2 = \frac{\log(15/3)}{\log(7/3)} = 1.465.$$

The corresponding numbers in the new two iterations are 1.694 and 1.834. These numbers point to the fact that the dimension of the geometry is still a fractional number, albeit approaching 2.

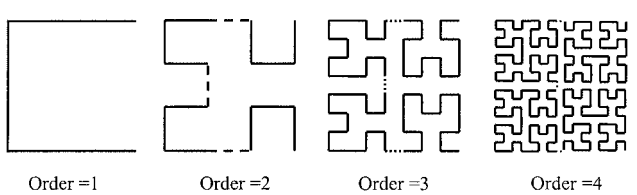

Figure 1 Generation of four iterations of Hilbert curves. The segments used to connect the geometry of the previous iteration are shown in dashed lines

As the dimension approaches 2, the curve is almost filling a plane. In other words, the total length of the line segments (with topological dimension 1) tends to be extremely large. This could lead to a significant advantage in antennas since the resonant frequency can be reduced considerably for a given area by increasing the fractal iteration order. It may be recalled that the dimension of this curve is larger than that of Koch curves (dimension = 1.262) studied elsewhere [8], resulting in a larger reduction factor for the antenna size. The studies presented here indicate that, by increasing the fractal iteration order, the resonant frequency of the antenna can be significantly reduced. Thus, this approach strives to overcome one of the fundamental limitations of antenna engineering with regard to small antennas [13]. It may, however, be notioned that, since fractals do not come under the purview of Euclidean geometry, stipulations based on this may be relaxed for fractals [11].

NUMERICAL SIMULATIONS

Numerical simulations were done using NEC, which is moment-method-based software. This is very effective in analyzing antennas that can be modeled with wire segments, such as the one under consideration here. The model gives accurate results when the segment length $< \lambda/20$. To suit the requirements, the antenna is modeled without any dielectric present, although some of the practical implementations do require dielectric support. A typical antenna geometry with a third iteration fractal curve is shown in Figure 2. This geometry is created with a recursive algorithm consistent with common fractal generation approaches. Since a reduction in the overall size of the antenna is of primary importance, this algorithm is implemented in such a way as to divide this into equal-sized segments. Thus, for a fractal geometry of third iteration in Figure 2 (nominal outer dimension = 7 cm $\times$ 7 cm), each line segment is of length 1 cm.

The feed source point is placed at the point of symmetry for these structures. The real and imaginary parts of the input impedance of this Hilbert curve fractal antenna with two, three, and four iterations are shown in Figure 3. The antennas occupy a square of side 2, 4, and 8 cm in these cases. Thus, an antenna with a third iteration fractal consists of four subgeometries occupying the same area as with the second iteration considered here. This shows the multiple resonance characteristics of the antenna, as well as the self-similarity of its characteristics.

To explore the extent of the plane-filling characteristics of the antenna geometry, these three iterations are also made within a uniform area of 7 cm $\times$ 7 cm, and the corresponding results are shown in Figure 4. These indicate the self-similarity in the antenna characteristics. Another important characteristic to be noticed is the lowest resonant frequency in each case. The resonant frequencies are for the third iteration: 360, 980, and 1440 MHz, and for the fourth iteration: 270, 720, 1000, and 1370 MHz. This shows a reduction in the resonant frequency (in this case by 25%) with an increase in the fractal iteration order, despite the outer dimensions of the antenna being the same. The predicted radiation patterns at the resonant frequencies for the third iterated fractal antenna at its resonant frequencies are shown in Figure 5. The geometry is placed in the *xy*-plane, and the pattern cuts are provided for all three orthogonal planes. These indicate that, at least for the first two resonances, the shape of the radiation pattern remains the same. This is in contrast to a normal dipole antenna where additional nulls appear with each subsequent resonances. The reason for this difference is that the overall size of this radiator remain considerably less than that of an equivalent linear dipole at these frequencies.

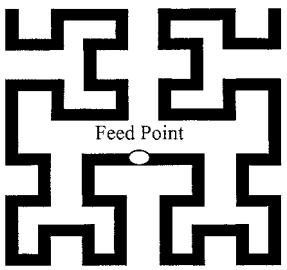

Figure 2 Antenna configuration with Hilbert curve fractal patterns, used in simulation

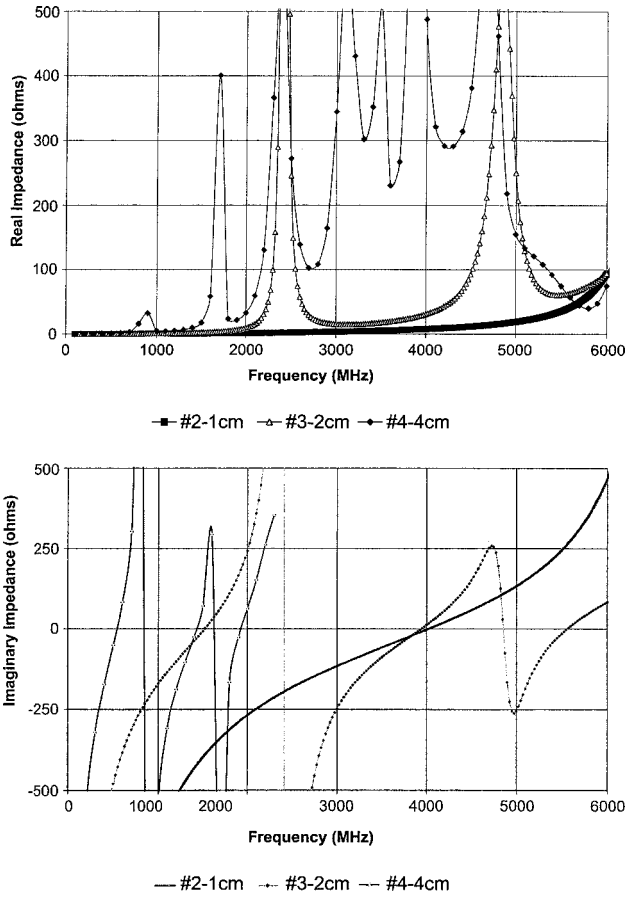

Figure 3 Real and imaginary parts of the input impedance for three iterations of Hilbert curve fractal antennas obtained with numerical simulations. The second resonant frequency for the third iterated curve is slightly lower than the resonant frequency for the second iterated curve. This may be due to the loading effects, in addition to the small connector segment added in the fractal generation. The imaginary part of the fourth iterated antenna shows many more resonances, and is truncated for clarity

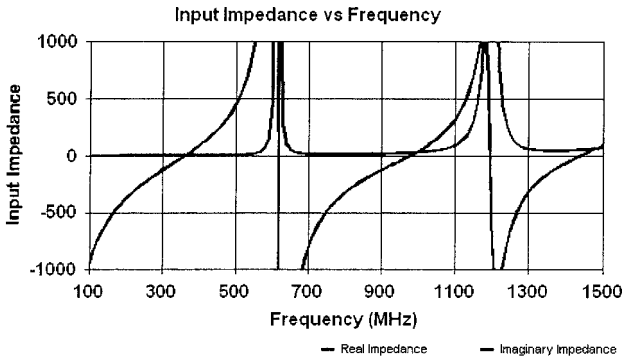

Figure 4 Computed input impedances for (a) third and (b) fourth iteration Hilbert curve antenna. Both antennas have outer dimensions of 7 cm, and are modeled with a wire of 1.3 mm diameter

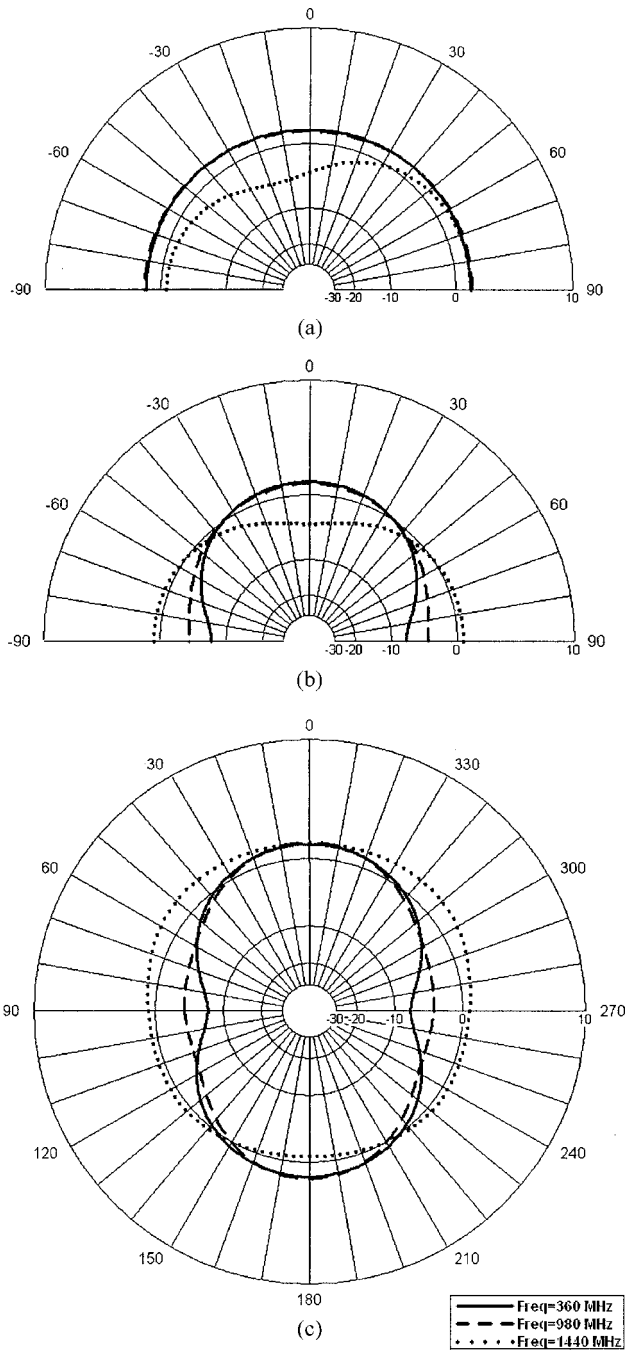

Figure 5 Predicted radiation pattern in two orthogonal planes intersecting the antenna geometry, at different resonant frequencies. The antenna geometry is in the *xy*-plane. The pattern cuts in the (a) *xz*-plane, (b) *yz*-plane, and (c) *xy*-plane are shown. The input impedance of the geometry used here is shown in Figure 4(a)

EXPERIMENTAL RESULTS

The NEC prediction for the third iteration antenna geometry has been compared with experimental results. The measured results for this antenna made with copper strips of 4 mm width are shown in Figure 6. The corresponding simulated results are presented in Figure 4(a). In the simulation, however, an equivalent wire diameter is used [14]. The slight mismatch in this is attributed to the feed arrangement being unbalanced. The low values for the real part of the impedance are consistent with other similar small antennas, such as Koch antennas [15] and small meander-line antennas [2]. However, by using impedance-matching circuits, or even by changing the feed location, this can be remedied.

CONCLUSIONS

The effect of self-similarity and plane-filling properties of fractal Hilbert curves in antenna characteristics is studied numerically using a moment-method-based software, and the predicted input characteristics are compared with experimental data. The results presented here establish the link between the self-similarity of the antenna geometries and its frequency response. Another important advantage of using Hilbert curves is the incorporation of its plane-filling characteristics to realize *resonant antennas* with a smaller overall physical size. A fourth iterated fractal Hilbert curve geometry inscribed in a square of side 7 cm is shown to result in a resonant frequency of 267 MHz, which is much lower than any other resonant antenna of similar size.

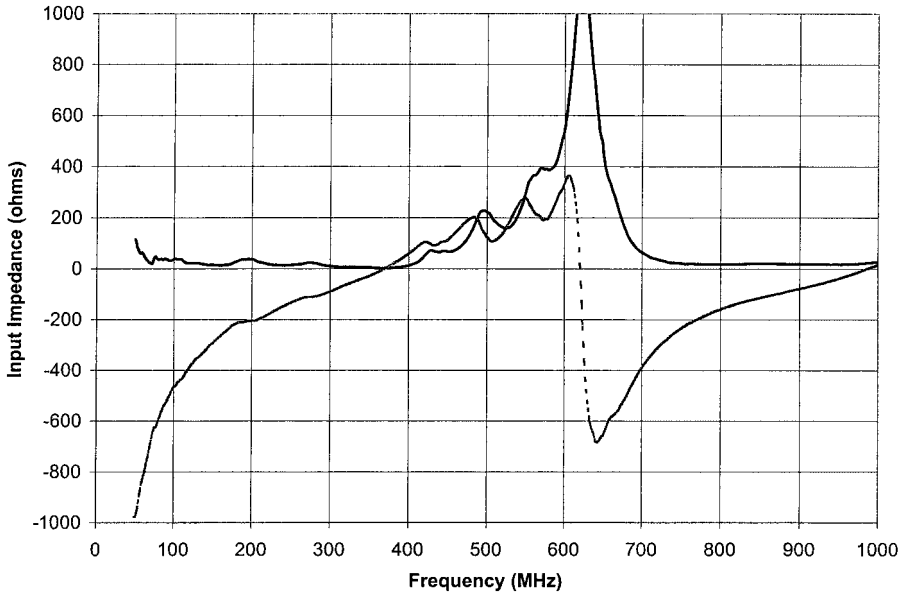

Figure 6 Measured input impedance of a Hilbert curve fractal antenna. The antenna is fabricated with 4 mm wide copper strips of the third iterated fractal geometry occupying a 7 cm square area. The measured performances of this antenna is comparable with the simulated response in Figure 4(a)

REFERENCES

1. H. Nakano, H. Tagami, A. Yoshizawa, and J. Yamauchi, Shortening ratios of modified dipole antennas, IEEE Trans Antennas Propagat AP-32 (1984), 385–386.
2. T.J. Warnagiris and T.J. Minardo, Performance of a meandered line as an electrically small transmitting antenna, IEEE Trans Antennas Propagat 46 (1998), 1797–1801.
3. B.B. Mandelbrot, The fractal geometry of nature, Freeman, New York, 1983.
4. D.L. Jaggard and T. Spielman, Triadic cantor target diffraction, Microwave Opt Technol Lett 5 (1992), 460–466.
5. A. Lakhtakia, N.S. Holter, V.K. Varadan, and V.V. Varadan, Self-similarity in diffraction by a self similar fractal screen, IEEE Trans Antennas Propagat AP-35 (1987), 236–239.
6. D.H. Werner, R.L. Haupt, and P.L. Werner, Fractal antenna engineering: The theory and design of fractal antenna arrays, IEEE Antennas Propagat Mag 41 (1999), 37–59.
7. C. Puente-Baliarda, J. Romeu, R. Pous, and A. Cardama, On the behavior of the Sierpinski multiband fractal antenna, IEEE Trans Antennas Propagat 46 (1998), 517–524.
8. N. Cohen, Fractal antenna applications in wireless telecommunications, Prof Program Proc Electron Ind Forum, Boston, MA, May 1997, pp. 43–49.
9. C. Puente-Baliarda, M. Navarro, J. Romeu, and R. Pous, Variations on the fractal Sierpinski antenna flare angle, IEEE AP-S Int Symp Dig, 1998, pp. 2340–2344.
10. V.K. Varadan, K. Vinoy, J.A. Kollakompil, and V.V. Varadan, Miniaturized conformal octave-bandwidth fractal antennas on high dielectric substrates and chiral layers, U.S. Patent application pending, July 2000.
11. C. Puente, J. Romeu, and A. Carsama, "Fractal shaped antennas," Frontiers in electromagnetics, D.H. Werner and R. Mittra (Editors), IEEE Press, New York, 1999, chap. 2.
12. H.O. Peitgen, H. Jurgens, and D. Saupe, Chaos and fractals: New frontiers of science, Springer-Verlag, New York, 1992.
13. R.C. Hansen, Fundamental limitations in antennas, Proc IEEE 69 (1981), 170–182.
14. C.A. Balanis, Antenna theory: Analysis and design, Wiley, New York, 1997, 2nd ed.
15. C. Puente-Baliarda, J. Romeu, R. Pous, J. Ramis, and A. Hijazo, Small but long Koch fractal monopole, Electron Lett 34 (1998), 9–10.

THREE-PORT RECTANGULAR MICROSTRIP UNEQUAL POWER DIVIDER AND COUPLER

Sudhabindu Ray[1] and Girish Kumar[1]
[1] Department of Electrical Engineering
Indian Institute of Technology, Bombay
Powai, Mumbai 400 076, India

Received 16 November 2000

ABSTRACT: *A new configuration of a three-port rectangular microstrip power divider and coupler has been proposed. It can easily implement unequal power division of a large ratio, i.e., the power coupled to the third port can vary from −3 to −26 dB. The configuration has been analyzed using a transmission-line model, as well as method-of-moments-based software.* © 2001 John Wiley & Sons, Inc. Microwave Opt Technol Lett 29: 219–223, 2001.

Key words: *rectangular microstrip power divider; coupler*

1. INTRODUCTION

Power dividers and couplers are the building blocks of microwave and millimeter-wave systems. In a planar configuration, the branch-line directional coupler was first proposed by Reed and Wheeler in 1956 [1], and the *n*-way power divider was reported by Wilkinson in 1960 [2]. After that, several types of power dividers and couplers, including direct-coupled and coupled-line configurations, were reported [3–11]. An unequal power divider can be realized by using a two-way